ISPRS Journal of Photogrammetry and Remote Sensing 144 (2018) 1–13

Contents lists available at ScienceDirect

ISPRS Journal of Photogrammetry and Remote Sensing

journal homepage: www.elsevier.com/locate/isprsjprs

Estimation of the directional and whole apparent clumping index (ACI) from indirect optical measurements

Hongliang Fang*, Weiwei Liu, Wenjuan Li, Shanshan Wei

LREIS, Institute of Geographic Sciences and Natural Resources Research, Chinese Academy of Sciences, Beijing 100101, China
University of Chinese Academy of Sciences, Beijing 100049, China

ARTICLE INFO

Keywords:
Apparent clumping index (ACI)
Directional ACI
Whole ACI
Leaf area index (LAI)
Optical instruments
Rice

ABSTRACT

Canopy clumping index (CI) indicates the non-random distribution of foliage components in space, and is an important structural parameter for better understanding the radiative transfer process in a canopy. The apparent clumping index (ACI), calculated using the logarithmic gap fraction averaging method, is reported by the LAI-2200 Plant Canopy Analyzer. While LAI-2200 calculates the gap fraction and ACI from different conical rings, calculation of ACI for other geometric units (e.g., an angular cell or an azimuth sector) and instruments has been lacked. Building upon the LAI-2200 ACI, this study compares the ACIs calculated for different geometric spaces from different optical instruments. The field data obtained from seasonal continuous measurements with LAI-2200, digital hemispheric photography (DHP), and AccuPAR at a paddy rice field in northeast China were used to calculate the directional ACIs at different levels—a directional cell ($\Omega_A(\theta, \phi)$), a concentric ring ($\Omega_A(\theta)$), an azimuth sector ($\Omega_A(\phi)$), and over the horizontal landscape ($\Omega_A(\nu)$). The whole ACIs were calculated from the directional ACIs with an angular integration method, a simple averaging method, a non-linear correction method, and a variance-to-mean ratio method. The directional ACIs for paddy rice generally follow the order of $\Omega_A(\theta, \phi) < \Omega_A(\theta)$ and $\Omega_A(\phi) < \Omega_A(\nu)$, displaying an increase of foliage randomness with the segment size. The $\Omega_A(\theta, \phi)$ estimated from DHP indicates canopy clumping at the finest level and is consistent with the CIs estimated from the logarithmic averaging method (Ω_{LX}) and the ratio method (the effective leaf area index (LAI_e) divided by the LAI). The ACI metrics expand the current CI metrics and can be obtained with different optical instruments. The expanded metrics can be applied in the canopy radiative transfer modeling and in the estimation of canopy biophysical parameters for other vegetation ecosystems.

1. Introduction

The spatial distribution of canopy foliage elements, generally described by a clumping index (CI), is important for proper understanding of canopy radiative transfer, precipitation interception, and the photosynthetic process (Wei and Fang, 2016). In theory, CI (Ω) is defined as the ratio of the effective leaf area index (LAI_e), usually obtained by optical sensors, to the true leaf area index (LAI) (Nilson, 1971; Fernandes et al., 2014)

$$\Omega = LAI_e/LAI \quad (1)$$

The value of CI is equal to 1.0 when leaves are randomly distributed, and less than 1.0 when leaves are aggregated. CI has been incorporated in several land surface models (LSMs) to characterize the radiation penetration and photosynthetic processes in clumped canopies (Chen et al., 2012; Haverd et al., 2012; Ni-Meister et al., 2010; Nouvellon et al., 2000; Pinty et al., 2006; Rambal et al., 2003; Yang et al., 2010). The gross primary productivity (GPP) and canopy evapotranspiration (ET) would be substantially underestimated if LAI_e is used without taking CI into consideration (Chen et al., 2016, 2012).

Global and regional scale CI products have been generated from POLDER, MODIS, and MISR satellite data, based on an empirical relationship with the normalized difference between hotspot and darkspot (NDHD) (Chen et al., 2005; Leblanc et al., 2005b). The monthly POLDER CI was generated at 6 km resolution from October 1996 to June 1997 and the minimum CI during the eight months was extracted as the final product (Chen et al., 2005). The global MODIS CI was estimated from NDHD at 500 m resolution, and the seasonal variability was explored at a regional scale (He et al., 2012; He et al., 2016). Moreover, the MISR CI was derived with a similar method at a regional scale in 275 m (Pisek et al., 2013).

Commercial optical instruments, e.g., digital camera (Ryu et al., 2012), digital hemispheric photography (DHP) (Fang et al., 2014; Leblanc et al., 2005a; van Gardingen et al., 1999), LAI-2200 (Fang

* Corresponding author at: LREIS, Institute of Geographic Sciences and Natural Resources Research, Chinese Academy of Sciences, Beijing 100101, China.
E-mail address: fanghl@lreis.ac.cn (H. Fang).

https://doi.org/10.1016/j.isprsjprs.2018.06.022
Received 13 February 2018; Received in revised form 11 May 2018; Accepted 29 June 2018

et al., 2014, 2018), and TRAC (Chen and Cihlar, 1995), have been frequently used to take indirect CI estimates when making field LAI measurements. The choice of a specific method varies for different biome types and ground conditions (Demarez et al., 2008; Gonsamo and Pellikka, 2009; Pisek et al., 2011). In theory, CI is generally derived in the estimation of LAI_e with the Beer-Lambert equation (Nilson, 1971)

$$P(\theta) = e^{-G(\theta)\cdot LAI_e(\theta)/\cos(\theta)} = e^{-G(\theta)\cdot\Omega(\theta)\cdot LAI/\cos(\theta)} \quad (2)$$

where θ is the solar zenith angle, $P(\theta)$ is the canopy gap fraction in direction θ, and $G(\theta)$ is the foliage projection function. Miller (1967) proposed a theorem for the inverse estimation of LAI_e that does not require a prior knowledge of $G(\theta)$.

$$LAI_e = 2\int_0^{\pi/2} -\ln P(\theta)\cos\theta\sin\theta d\theta \quad (3)$$

When multiple observations of $P(\theta)$ are available, there are two averaging methods ($\ln\overline{P(\theta)}$ vs. $\overline{\ln P(\theta)}$) and Eq. (3) can be expressed as:

$$L_1 = 2\int_0^{\pi/2} -\ln\overline{P(\theta)}\cos\theta\sin\theta d\theta \quad (4)$$

or

$$L_2 = 2\int_0^{\pi/2} -\overline{\ln P(\theta)}\cos\theta\sin\theta d\theta \quad (5)$$

CI can be derived as a ratio of the above two equations:

$$\Omega = L_1/L_2 = \frac{\int_0^{\pi/2} -\ln\overline{P(\theta)}\cos\theta\sin\theta d\theta}{\int_0^{\pi/2} -\overline{\ln P(\theta)}\cos\theta\sin\theta d\theta} \quad (6)$$

Eq. (6) can be expressed in a simple numerical form:

$$\Omega = \frac{\ln\overline{P}}{\overline{\ln P}} \quad (7)$$

The logarithmic averaging equation (Eq. (7)), i.e., the LX method, is calculated over different segments (Lang and Xiang, 1986) and thus the size of segments significantly affect the CI values estimated using this method (Demarez et al., 2008; Pisek et al., 2011). The segment size should be large enough so that the statistics of the gap fraction are meaningful, and small enough for the assumption of leaf distribution randomness within a cell to hold. Demarez et al. (2008) experimented with different segment sizes and found that $10^\circ \times 16^\circ$ is optimal for corn fields. Pisek et al. (2011) suggested a 15° DHP interval to be compatible with the TRAC measurement. Theoretically, the most appropriate gap fraction sampling size is related to pixel size and angular units (Gonsamo et al., 2010). However, the determination of the optimal sampling resolution for various canopy types is not trivial. A theoretical analysis of this problem suggests that a segment of at least 10 times the width of a leaf should be used (Lang, 1986; Leblanc et al., 2005a).

For the commonly used instruments, the observational configuration and the segment size cannot be directly compared, and problems arise in the interpretation of CIs obtained from different optical instruments (Fang et al., 2014; Ryu et al., 2010b). DHP provides a fine sampling of segments that can be used to derive CI at different levels. The LAI-2200 gap fractions are derived from the transmittance observations at different rings. Without a view cap restriction, it is impossible to mimic the DHP cells because LAI-2200 provides an azimuthally integrated transmittance for each ring. In an entirely different manner, AccuPAR and other ceptometers make photosynthetically active radiation (PAR) observations over a whole hemisphere (Decagon Devices, 2004).

Ryu et al. (2010a) coined an apparent clumping index (ACI) for LAI-2200, calculated in the form of Eq. (6), where $P(\theta)$ is calculated for each ring. The purpose of ACI is to compensate for the clumping factor inherent in LAI-2200 rings and to properly calculate the true LAI (LI-COR, 2010; Ryu et al., 2010a).

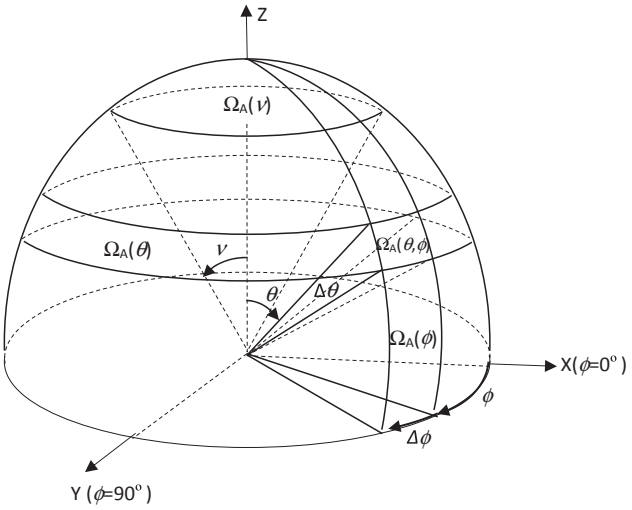

Fig. 1. Schematic illustration of different ACI metrics for different geometric units over the upper hemisphere. $\Omega_A(\theta, \phi)$ represents canopy clumping at direction (θ, ϕ). $\Omega_A(\theta)$ and $\Omega_A(\phi)$ are for a certain annulus or an azimuth sector, and $\Omega_A(\nu)$ over a solid angle ν.

$$LAI = \frac{LAI_e \times ACI}{\Omega} \quad (8)$$

where Ω is an independently determined clumping index, for example, from a gap size distribution measurement (Chen and Cihlar, 1995). Currently, LAI-2200 is the only instrument that reports ACI. Nevertheless, the ACI reported in LAI-2200 has rarely been investigated by the community.

Over the space, LAI-2200 calculates the gap fraction $P(\theta)$ and ACI ($\Omega_A(\theta)$) for five concentric conical rings only (Fig. 1). Other optical instruments provide more diversified spacial sampling and can be used to calculate various ACIs to describe the enhanced foliage distribution information. For example, DHP samples the field with a high angular resolution that can be used to calculate the gap fraction at an angular cell $P(\theta, \phi)$, an azimuth sector $P(\phi)$, or a solid angle $P(\nu)$ (Fig. 1). These instruments would enhance our existing knowledge about ACI and expand the conventional CI concept.

This paper aims to expand the ACI concept to other geometric units and instruments. We examined the variation of the directional CI at the cell level and the zenith and azimuth distribution of the ACI. The study addresses two crucial questions: (1) what are the zenith and azimuth distributions of the directional CI, and (2) what are the characteristics of the whole ACI estimated from different optical instruments. We address these questions through theoretical derivation and an experiment conducted in the paddy rice fields in northeast China.

2. Methods and material

2.1. Comparison of CI at the cell level

Generally, it is assumed that the leaf orientation is randomly distributed along the azimuth angle (ϕ) and CI is independent of ϕ. This assumption might not be true for row crops because of the large gaps between rows (Drouet and Moulia, 1997; Sinoquet and Andrieu, 1993). In this case, $P(\theta, \phi)$ needs to be calculated for a particular viewing cell, specified by the angular increment $(\Delta\theta, \Delta\phi)$ (Fig. 1). Similar to Eq. (7), a directional ACI is defined for (θ, ϕ) (Lang and Xiang, 1986):

$$\Omega_A(\theta, \phi) = \frac{\ln\overline{P(\theta,\ \phi)}}{\overline{\ln P(\theta,\ \phi)}} \quad (9)$$

where $\Omega_A(\theta, \phi)$ describes the non-random distribution of foliage at a particular angular location (θ, ϕ) and size $(\Delta\theta, \Delta\phi)$. Among the common indirect methods, DHP has very fine view zenith and azimuth

resolutions over a range of angles, either simultaneously or through multiple measurements, to provide estimates of gap fractions and $\Omega_A(\theta, \phi)$ at a particular segment.

2.2. The directional ACI

In a similar fashion, gap fractions $P(\theta)$ and $P(\phi)$ can be calculated at a conical ring ($\Delta\theta$) or an azimuth sector ($\Delta\phi$), respectively (Fig. 1). In this case, ACI can be calculated from gap fractions at the zenith or azimuth angles.

$$\Omega_A(\theta) = \frac{\ln \overline{P(\theta)}}{\overline{\ln P(\theta)}} \tag{10}$$

$$\Omega_A(\phi) = \frac{\ln \overline{P(\phi)}}{\overline{\ln P(\phi)}} \tag{11}$$

$\Omega_A(\theta)$ and $\Omega_A(\phi)$ describe the foliage clumping at a particular zenith ring or an azimuth sector. For DHP images, $P(\theta)$ and $P(\phi)$ can be calculated by integrating $P(\theta, \phi)$ for a specific angular unit ($\Delta\theta$ or $\Delta\phi$). For LAI-2000, gap fractions $P(\theta)$ are directly convolved into five discrete conical rings centered at 7°, 23°, 38°, 53°, and 68°, respectively (Appendix A.1). The $\Omega_A(\theta)$ for different rings and the whole Ω_A as a weighted average of all rings are reported in the LAI-2200 standard data file (labeled ACFS) (LI-COR, 2010).

Finally, $P(\nu)$ can also be computed as the canopy openness over all azimuth angles from a specified zenith angle (ν) to nadir. Similarly, the $\Omega_A(\nu)$ is given to quantify the canopy non-randomness in the horizontal direction by

$$\Omega_A(\nu) = \frac{\ln \overline{P(\nu)}}{\overline{\ln P(\nu)}} \tag{12}$$

For brevity purpose, angle ν was used to represent the viewing field, while the actual solid angle would be 4ν for a conical field of view (FOV) (Fig. 1). $\Omega_A(\nu)$ can be calculated from DHP over any ν angle larger than the pixel size. For LAI-2200, $\Omega_A(\nu = 12.3°)$ is numerically equal to $\Omega_A(\theta)$ for the first ring. $\Omega_A(\nu)$ values for other FOVs can be calculated from concurrent above and below canopy readings. Moreover, $P(\nu)$ and $\Omega_A(\nu)$ can be directly calculated from AccuPAR ($\nu = 90°$).

2.3. Calculation of the whole ACI

2.3.1. Angular integration (INT) method

Eq. (2) can be expressed as

$$-\ln P(\theta)\cos(\theta) = G(\theta)\Omega(\theta)\mathrm{LAI} \tag{13}$$

which can then be included in Eq. (3) to estimate $\mathrm{LAI_e}$

$$LAI_e = 2\int_0^{\pi/2} G(\theta)\Omega(\theta)\mathrm{LAI}\sin\theta d\theta \tag{14}$$

With Eq. (1), the whole clumping index Ω can be derived as an integration of the directional $\Omega(\theta)$ (Stenberg et al., 2014).

$$\Omega_{\mathrm{INT}} = 2\int_0^{\pi/2} \Omega(\theta)G(\theta)\sin\theta d\theta \tag{15}$$

2.3.2. Simple angular averaging (AVG) method

For simplicity, the whole ACI can be calculated as an average of angular $\Omega(\theta)$ values (Duthoit et al., 2008; Fang et al., 2014):

$$\Omega_{\mathrm{AVG}} = \frac{1}{N}\sum_{i=1}^{N}\Omega(\theta_i) \tag{16}$$

where N is the number of angular sectors.

2.3.3. Non-linear correction (NLC) method

Ryu et al. (2010a) applied a second order Taylor's expansion for the average of the logarithmic gap fraction:

$$-\overline{\ln P(\theta)} \approx -\ln \overline{P(\theta)} - \frac{1}{2}(\ln \overline{P(\theta)})'' S(P(\theta)) \tag{17}$$

The second term in the right includes the second derivate of logarithm ($= -1/[\overline{P(\theta)}]^2$) and the variance of gap fraction $S(P(\theta))$. Therefore, Eq. (17) can be expressed as:

$$\int_0^{\pi/2} -\overline{\ln P(\theta)}\cos\theta\sin\theta d\theta \approx \int_0^{\pi/2} -\ln \overline{P(\theta)}\cos\theta\sin\theta d\theta + \frac{1}{2}\int_0^{\pi/2} \frac{S(P(\theta))}{[\overline{P(\theta)}]^2}\cos\theta\sin\theta d\theta \tag{18}$$

In Ryu et al. (2010a), the second term on the right hand side of Eq. (18) is named as a non-linearity correction (NLC) term. Thus, the whole ACI can be approximated by:

$$\Omega_{\mathrm{NLC}} \approx 1 - 0.5\frac{\int_0^{\pi/2} S(P(\theta))/[\overline{P(\theta)}]^2\cos\theta\sin\theta d\theta}{\int_0^{\pi/2} -\overline{\ln P(\theta)}\cos\theta\sin\theta d\theta} \tag{19}$$

2.3.4. Simple variance to mean ratio (VMR) of the lnP(θ)

The variance-to-mean ratio (VMR) is a commonly used measure of the degree of randomness in probability theory and statistics. It has been used to quantify the degree of forest stem clumping for a given quadrat (Woodgate et al., 2016). The VMR method is slightly altered so most of the values are between 0 and 1.

$$\Omega_{\mathrm{VMR}}(\theta) = 1 - \frac{S[\ln P(\theta)]}{-\overline{\ln P(\theta)}} \tag{20}$$

where S is the variance of $\ln P(\theta)$ and is expressed by:

$$S[\ln P(\theta)] = \sqrt{\frac{\sum_{i=1}^{n}[\ln P_i(\theta) - \overline{\ln P(\theta)}]^2}{n-1}} \tag{21}$$

Following Eq. (15), the whole clumping index Ω_A is thus an integration of the directional $\Omega_{\mathrm{VMR}}(\theta)$:

$$\Omega_{\mathrm{VMR}} = 2\int_0^{\pi/2} \Omega_{VMR}(\theta)G(\theta)\sin\theta d\theta \tag{22}$$

2.3.5. Comparison with the conventional CI

The commonly used LX method calculates CI for different zenith angles with the following equation (Fang et al., 2014; Weiss and Baret, 2014):

$$\Omega_{\mathrm{LX}}(\theta) = \frac{\ln \overline{P(\theta,\ \phi)}}{\overline{\ln P(\theta,\ \phi)}} \tag{23}$$

$\Omega_{\mathrm{LX}}(\theta)$ is calculated from all cellular gap fraction $P(\theta, \phi)$ over an entire angle θ. The $\Omega_{\mathrm{LX}}(\theta)$ was compared with the whole ACIs calculated from the four different methods above. It is noteworthy that the $\Omega_{\mathrm{LX}}(\theta)$ in Eq. (23) is different from that in Eq. (10) as $P(\theta, \phi)$ and $P(\theta)$ are calculated over different geometric units. For a single image, Ω_{LX} is estimated in a similar fashion (Leblanc et al., 2005a; van Gardingen et al., 1999):

$$\Omega_{LX} = \frac{\ln \overline{P(\theta,\ \phi)}}{\overline{\ln P(\theta,\ \phi)}} \tag{24}$$

where $P(\theta, \phi)$ is calculated for each segmented cell in the image. This equation is similar to Eqs. (7) and (9) but is calculated for all cells in one image.

2.4. Data and analysis

Field data obtained from the Paddy Rice Experiment in the Sanjiang Plain (PRESP) were used in this study (Fang et al., 2014). The field campaign was carried out at the Honghe Farm (47°39′ N, 133°31′ E), Heilongjiang province, northeast China, from June 11 to September 17,

Table 1
Location of the five plots and instruments used in the study.

Plot	Latitude	Longtitude	Plant density (plants/m^2)	Row space (cm)
A	47.667°N	133.515°E	25	28.8
B	47.663°N	133.532°E	26	28.6
C	47.653°N	133.523°E	24	29.9
D	47.637°N	133.515°E	28	28.3
E	47.637°N	133.534°E	28	27.4

2012 (Fang et al., 2014). Rice is usually transplanted in late May and harvested in late September in the area. Five plots (A, B, C, D, and E) were selected and intensive field data were collected following the good practices for LAI validation (Fernandes et al., 2014). The distances between rows and plants were measured five times randomly within an elementary sampling unit (ESU) (Table 1). Indirect optical LAI measurements were taken using DHP, LAI-2200, and AccuPAR throughout the growing season until the rice was near harvest. All measurements were conducted near sunset or under overcast conditions to minimize the error under direct illumination (Demarez et al., 2008; Garrigues et al., 2008). The rice height, water depth, and sky conditions in different crop growth stages are provided in Table S1 of the supplementary online material (SOM).

The DHP images were taken using a Nikon D5100 camera and a 4.5 mm F2.8 EX DC circular fisheye converter. The total height of the camera and the lens were about 16.5 cm. The fisheye camera was calibrated before the experiment using the method described in the CAN_EYE manual (version 6.3.3) (Weiss and Baret, 2010). An ultraviolet cap was used to protect the lens and two bubble levels were attached to the camera to keep it horizontal. Only downward-looking photos were taken before July 10 (DOY 192), when the rice entered the flowering stage. When the rice grew higher than 70 cm (after July 10), upward-looking photos were also taken together with the downward measurements at the same location. For the downward measurements, the camera was about 0.8–1.5 m above the canopy. For the upward measurements, the camera was placed right above the ground soil or water. Before July 26 (DOY 208), the camera was set to automatic exposure to avoid the saturation issues during the downward measurement (Demarez et al., 2008). After that, the aperture and shutter speed of the camera were manually adjusted to avoid overexposure during the shift from downward to upward measurements.

The DHP images were taken with a fixed azimuth angle to the row direction and were stored in JPEG format at a resolution of 3264 × 4928 pixels. The valid range of fisheye images was limited to a 60° zenith angle to avoid edge distortions. All images were reoriented to keep the row directions at 90° and 270°. The thresholding and classification were performed using the CAN-EYE software (version 6.3.3) (Weiss and Baret, 2014). In an interactive window, the operator selects color classes that correspond to either the green vegetation or the background. A thresholding method was then applied to separate the foliage from the soil background (downward view) or the sky (upward view). The classified images were divided into equiangular cells both in zenith and azimuth directions at a resolution of 10° (Fig. 2). The gap fraction $P(\theta, \phi)$ and $\Omega_A(\theta, \phi)$ were calculated (Eq. (9)) for each cell from all photographs taken within an ESU excluding the masked pixels. Gap fractions $P(\theta)$, $P(\phi)$, and $P(\nu)$ and the corresponding $\Omega_A(\theta)$, $\Omega_A(\phi)$, and $\Omega_A(\nu = 60°)$ at all levels were consequently calculated using the equations described in Section 2.2 (Fig. 3).

LAI-2200 (LI-COR Inc., Lincoln, Nebraska, USA) records the light penetration into the canopy at five concentric conical rings. Each measurement was repeated twice, with one above canopy and four below canopy readings. A 270° view cap was used to shield the sensor from the operator. The angular $\Omega_A(\theta)$ was calculated for each ring (Eq. (10)), and the whole ACI reported in the LAI-2200 data file was extracted. $\Omega_A(\nu)$ for the largest FOV ($\nu = 74.1°$) can be calculated as:

$$\Omega_A(\nu = 74.1°) = \frac{\ln\left(\frac{1}{N}\cdot\sum_{j=1}^{N}\left(\sum_{i=1}^{5}B_{ij}/\sum_{i=1}^{5}A_{ij}\right)\right)}{\frac{1}{N}\cdot\sum_{j=1}^{N}\ln\left(\sum_{i=1}^{5}B_{ij}/\sum_{i=1}^{5}A_{ij}\right)} \quad (25)$$

where the subscripts i and j refer to the number of rings ($i = 1 \ldots 5$) and observational pairs ($j = 1 \ldots N$), and B_{ij} and A_{ij} are the jth below and above canopy readings for ring i, respectively. $\Omega_A(\nu)$ for other viewing sky regions ($\nu = 12.3°$, $28.6°$, $43.4°$, and $58.6°$) can be calculated in a similar fashion.

Decagon's AccuPAR model LP-80 PAR/LAI ceptometer measures PAR values by locating the probe (FOV: 90°, length: 86.5 cm) below and above the canopy (Decagon Devices, 2004). The gap fraction $P(\nu)$ was calculated as the ratio of the transmitted PAR below the canopy to that above the canopy, and $\Omega_A(\nu)$ was calculated following Eq. (12). Moreover, the whole ACI values were calculated for DHP and LAI-2200 with the methods in Section 2.3. An example of the detailed ACI estimation from different instruments was given in the SOM (Text S1). All symbols used in the paper are listed in Appendix A.2.

Destructive LAI measurements were conducted by harvesting five bundles of rice in each ESU. The crops were taken to the laboratory in a cooler box and the areas of green leaves, stems, and ear components were measured with a LI-3100C leaf area meter (LI-COR Inc., Lincoln, Nebraska, USA) or a scanner when the stems were too thick. For all non-flat elements (stems, ears, and rolled leaves), the projected area was estimated. The destructive LAI is actually a plant area index (PAI) since all green and yellow leaves and stems were accounted for. By definition, the CI was calculated as a ratio of the optically estimated LAI_e to the destructive LAI (Eq. (1)).

3. Results

3.1. Comparison of ACIs at the cell level

Fig. 4 shows the seasonal variation of $\Omega_A(\theta, \phi)$ at the cell level retrieved from both downward and upward DHPs. The downward DHP shows that the $\Omega_A(\theta, \phi)$ generally decreases from 0.93 to lower than 0.80 around day-of-year (DOY) 205 (July 23) and increases to around 0.85 on DOY 241 (August 28) (Fig. 4a). Across the view angles, the $\Omega_A(\theta, \phi)$ values are generally lower in the nadir direction (0–10°), slightly increase between 10 and 30°, but behave erratically for 30–60° (Table 2). The $\Omega_A(\theta, \phi)$ values from the upward DHP are similar within 10–60°, varying between 0.72 and 0.78 from DOY 201 (July 19) to 230 (August 17) and are much more stable than the 0–10° values (Fig. 4c). The very low value in 0–10° is related to the extremely low value in plots C & D (Table 2).

Calculated for typical azimuth sectors, the downward DHP shows that the $\Omega_A(\theta, \phi)$ generally decreases from around 0.90 to around 0.80 on DOY 206 (July 24) and increases again to over 0.86 around DOY 240 (Fig. 4b). The downward $\Omega_A(\theta, \phi)$ values at the row direction (260–280°) are slightly lower (~0.05) than the values of the other directions before DOY 230 (Fig. 4b). The upward DHP shows more scattered $\Omega_A(\theta, \phi)$ variations (~0.10) at different azimuth angles. A slight increasing trend is visible from DOY 201 to DOY 240 (August 27) but the trend decreases after DOY 240 (Fig. 4d). Unlike the downward DHP, the upward $\Omega_A(\theta, \phi)$ values are higher in the 260–280° direction than the cross-row directions (350–10° and 170–190°).

3.2. Seasonal variation of the directional ACI

3.2.1. $\Omega_A(\theta)$ and $\Omega_A(\phi)$ estimated from DHP and LAI-2200

Fig. 5 shows the seasonal variation of $\Omega_A(\theta)$ and $\Omega_A(\phi)$ observed from the downward and upward DHPs, respectively. $\Omega_A(\theta)$ from the downward DHP decreases slightly during the peak growing season and increases during the senescent stage (Fig. 5a). The downward $\Omega_A(\theta)$ is

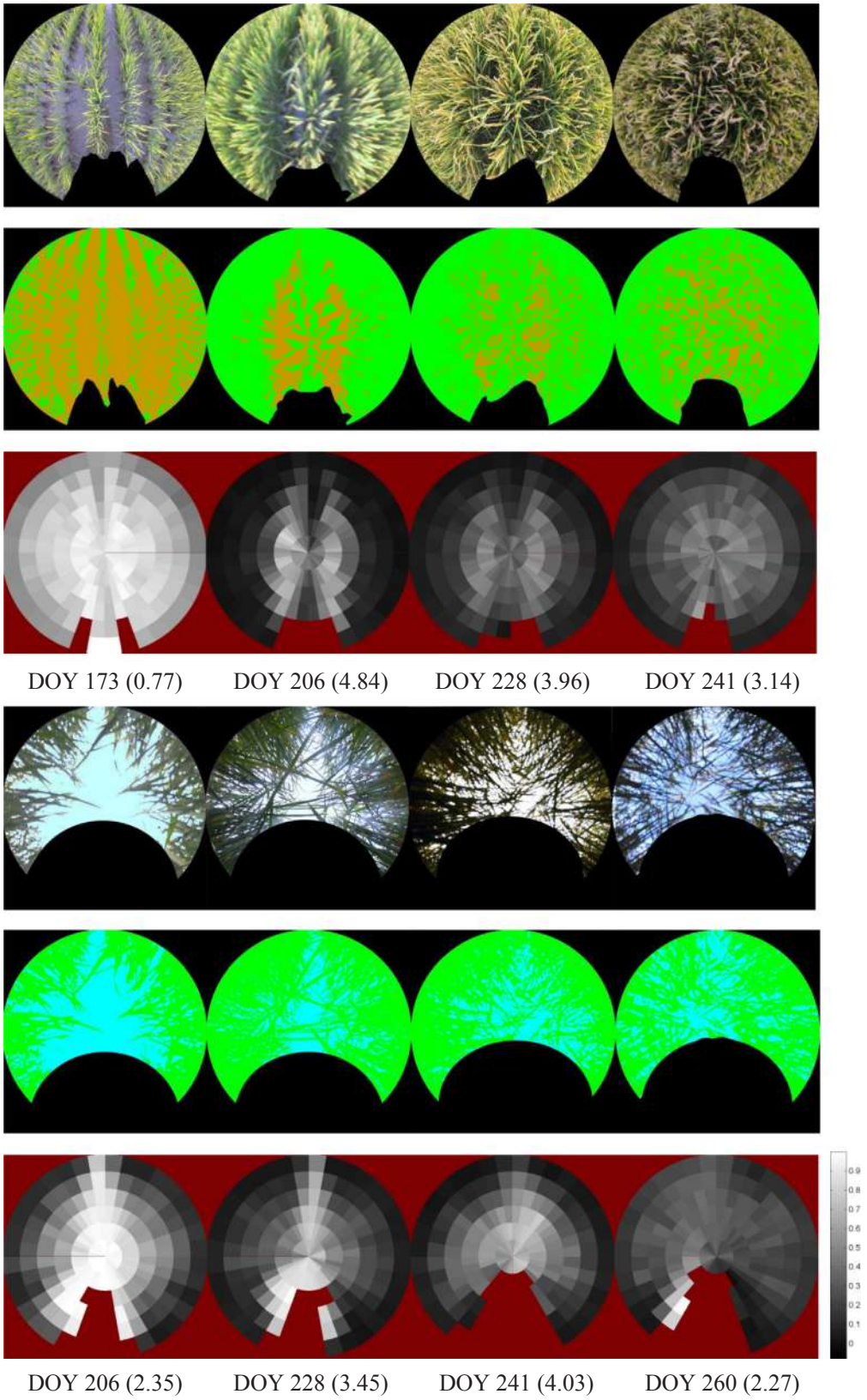

Fig. 2. Typical downward and upward DHP images, classification results, and gap fractions obtained on day-of-year (DOY) 173 (Jun 21), 206 (Jul 24), 228 (Aug 15), 241 (Aug 28), and 260 (Sep 16) in 2012. The number in brackets are the effective LAI values reported from LAI-2200.

lower for 0–10°, slightly increases between 10 and 40°, and decreases between 40 and 60° (Table 3). $\Omega_A(\theta)$ from the upward DHP shows no clear seasonal trend, but increases slightly with view angles (Table 3). For the downward DHP, Ω_A(0–10°) obtains some unusually lower (~0.05) values and decreases toward the end of the season.

The $\Omega_A(\phi)$ values from the downward DHP show very minor decreases (< 0.05) during the peak growing period (Fig. 5b). The $\Omega_A(\phi)$ values along the row direction (260–280°) are about 0.10 lower than

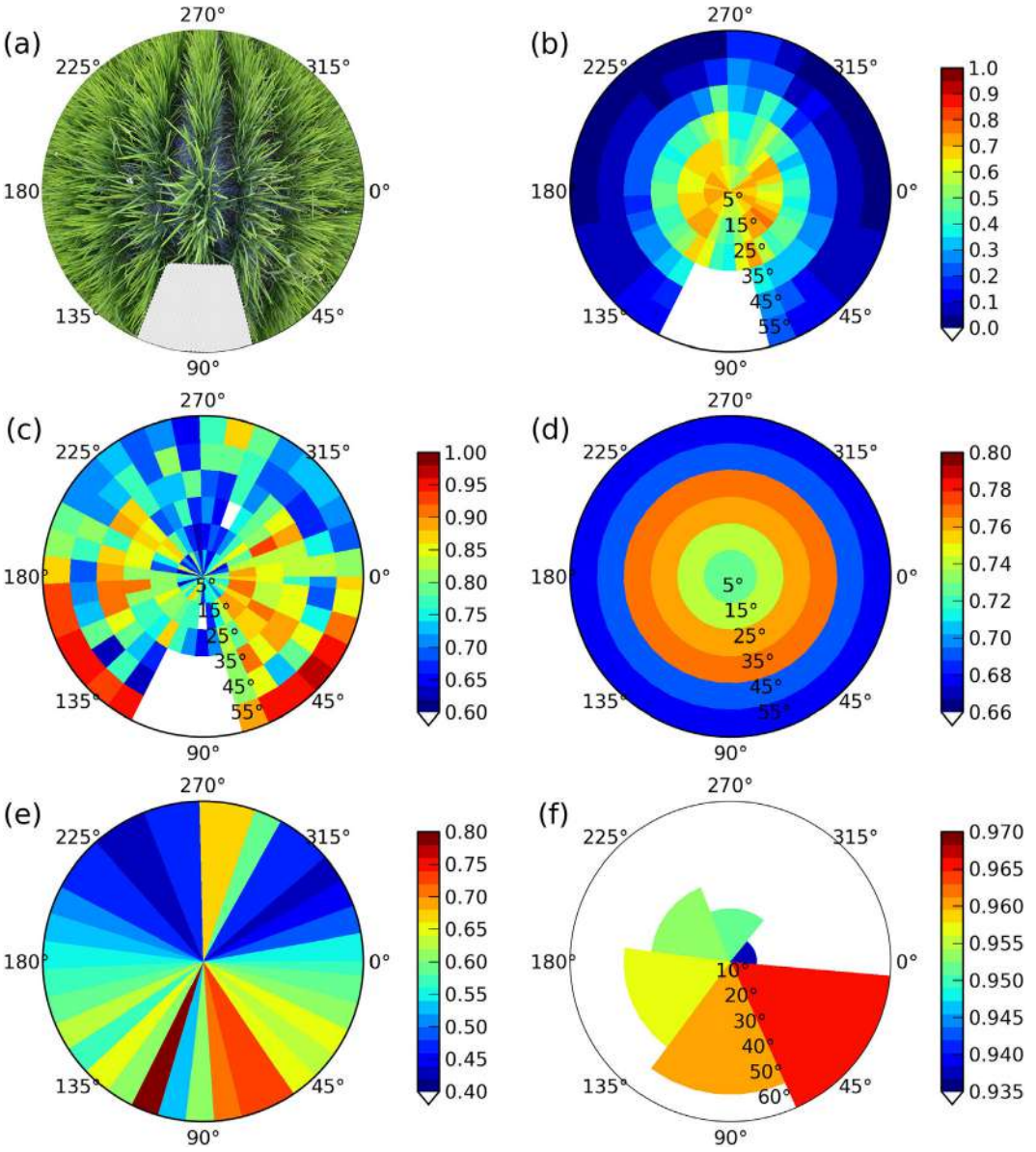

Fig. 3. A sample downward DHP image (a) and the gap fraction (b) over plot C on July 12, 2012 (DOY 194). Panels (c), (d), and (e) represent the $\Omega_A(\theta, \phi)$ values for each $10^\circ \times 10^\circ$ cell, $\Omega_A(\theta)$ for different rings, and $\Omega_A(\phi)$ for different azimuth sectors, respectively. Panel (f) indicates the $\Omega_A(\nu)$ values calculated over different solid angles (ν = 10–60°, respectively). Panels (c) – (f) are calculated over an ESU of 20 images.

the values of the other directions (Fig. 5b). The $\Omega_A(\phi)$ from the upward DHP shows a decreasing trend after DOY 200 (Fig. 5d). After DOY 230, the upward $\Omega_A(\phi)$ values in the cross-row and 310–320° directions are about 0.20 lower than those of the other two directions.

The $\Omega_A(\theta)$ values estimated by LAI-2200 are > 0.97 over the whole season (Fig. 6). The five rings show nearly identical $\Omega_A(\theta)$ values (~0.99) during the peak growing season between DOY 200 and 230. During the green-up period before DOY 205 (July 23), the $\Omega_A(\theta)$ values show a small decreasing trend with the viewing angles.

3.2.2. $\Omega_A(\nu)$ estimated from indirect optical methods

The $\Omega_A(\nu)$ estimated from DHP generally increases with the solid angle ν (Fig. 7a and b). The downward DHP shows a small decrease (~0.02) around DOY 190 (July 8) and a small increase around DOY 235 (August 22). The overall $\Omega_A(\nu)$ values are larger than 0.97 throughout the season (Fig. 7c). The DHP values are slightly smaller than those of the LAI-2200 and AccuPAR during the peak growing season. The small differences between the instruments are mainly attributed to the differences in the sensor field of view (60°, 74.1°, and 90° for DHP, LAI-2200, and AccuPAR, respectively).

3.3. Seasonal variation of the whole ACI

Fig. 8 compares the seasonal variation of the whole ACI calculated from $\Omega_A(\theta, \phi)$ using different methods. The downward DHP shows that the whole ACI decreases until DOY 205 (July 23) and slightly increases after that date. The whole ACI estimated from INT and AVG are nearly identical. The low valley of the NLC from DOY 201 to DOY 230 is related to the scattered values of $\Omega_A(\theta, \phi)$, especially at 0–10°. The upward DHP shows that the whole ACI slightly increases from DOY 201 to DOY 230 and decreases after that (Table 4). The VMR method shows a similar seasonal trend but the values are significantly lower. The negative Ω_{VMR} values are a result of the huge $\ln P(\theta)$ variance in Eq. (20).

Fig. 8 also shows the CIs calculated using the LX method (Ω_{LX}, Eq. (23)) and as a ratio of the optical LAI_e from DHP to the destructive LAI (Eq. (1)). $\Omega_A(\theta, \phi)$, Ω_{LX}, and $\Omega(LAI_e/LAI)$ values decrease with the

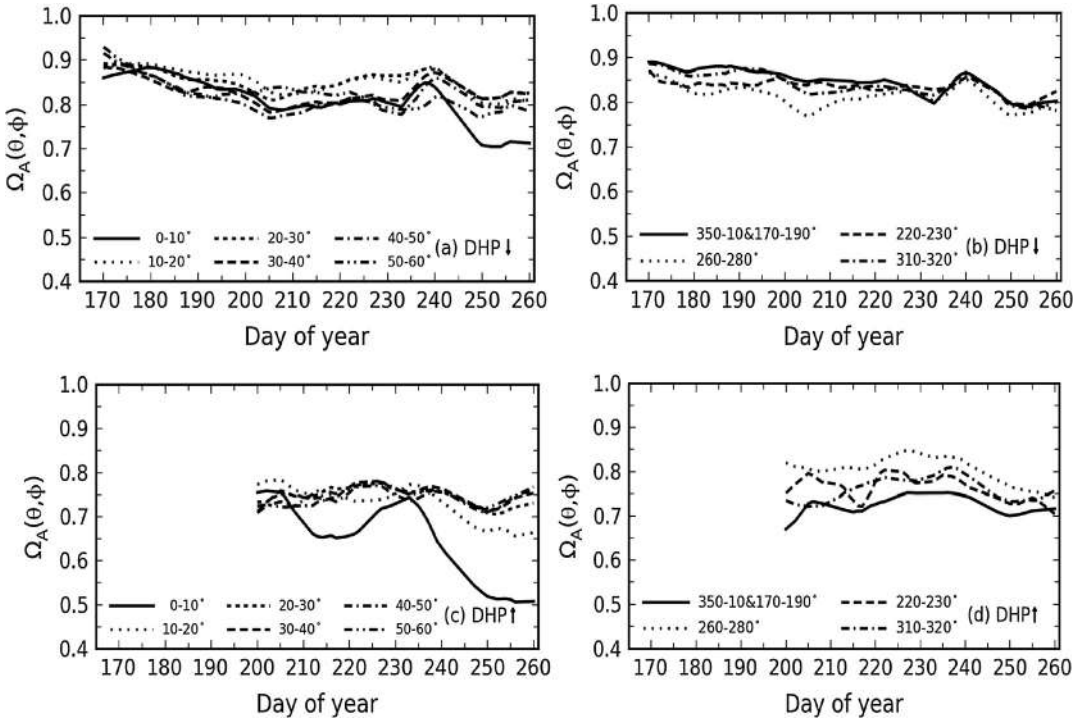

Fig. 4. Seasonal variation of $\Omega_A(\theta, \phi)$ estimated from the downward (upper panels) and upward (lower panels) DHP observations. Panels (a) and (c) show the $\Omega_A(\theta, \phi)$ values averaged over different zenith angles, and panels (b) and (d) over major azimuth angles. $\Omega_A(\theta, \phi)$ along 90° is not shown in (b) and (d) because of the operator shadow.

development of leaves and stems, remain low between DOY 191 (July 9) and 230 (August 17), and increase gradually toward the maturity stage (Table 4). The $\Omega_A(\theta, \phi)$ agrees with the Ω_{LX} in the middle of the season from DOY 201–230 but is slightly higher (~0.05) in the early and late parts of the season (Table 4). Ω_{LX} and $\Omega(LAI_e/LAI)$ are similar, but the $\Omega_A(\theta, \phi)$ values are slightly higher (~0.10) than Ω_{LX} and $\Omega(LAI_e/LAI)$ from DOY 191 to 230 (Table 4). The small differences are mainly attributed to the different ways in calculating the gap fraction distributions.

Fig. 9 compares the seasonal variation of the whole ACI calculated from the DHP and LAI-2200 $\Omega_A(\theta)$ values. The downward DHP shows a clear seasonal variation, with the ACI values decreasing during the middle of the season and increasing toward the end of the season. The seasonal ACI profiles from the upward DHP and LAI-2200 are more stable than those of the downward DHP. In general, the whole ACIs estimated from the AVG and NLC methods are similar to the INT method. The VMR method shows similar but larger seasonal variation compared to the other methods. From the downward DHP, the Ω_{NLC} is slightly smaller (~0.02) than the Ω_{INT} and the Ω_{AVG} during DOY 215–240. The whole ACI reported in LAI-2200 (Ω_A(LAI-2200)) increases swiftly during the green-up period and remains stable after DOY 201 (July 19). After DOY 201, all ACIs values are higher than 0.985 until the end of the season (Table 5).

4. Discussion

4.1. ACIs for different geometric spaces

4.1.1. Interpretation of the ACI metrics

ACI represents foliage clumping at different levels of geometrical space and is a more practical metric than the theoretical CI. Among the ACI metrics, $\Omega_A(\theta, \phi)$, $\Omega_A(\theta)$, and $\Omega_A(\phi)$ vary with the zenith and azimuth angles, while $\Omega_A(\nu)$ accounts for the non-random clustering of leaves across the landscape. $\Omega_A(\theta, \phi)$ indicates the foliage non-randomness for both zenith and azimuth directions. $\Omega_A(\theta)$ and $\Omega_A(\phi)$ are informative for a certain annulus or azimuth direction, yet are limited in revealing small gaps in the canopy. $\Omega_A(\nu)$ may display, to a large extent, the landscape horizontal homogeneity.

ACIs at various levels generally follow the order $\Omega_A(\theta, \phi) < \Omega_A(\theta)$ and $\Omega_A(\phi) < \Omega_A(\nu)$. The average $\Omega_A(\theta, \phi)$ values for a particular concentric angle θ are usually less than $\Omega_A(\theta)$ (Figs. 4 and 5), suggesting that the rice canopy is more clumped at a cell level than at the ring or

Table 2
The $\Omega_A(\theta, \phi)$ mean (standard deviation) values estimated from DHP for different view zenith angles (VZA) and day of the year (DOY). The last column is an average all angular values.

VZAs	0–10°	10–20°	20–30°	30–40°	40–50°	50–60°	Average
DHP downward							
DOY 170–200	0.845 (0.042)	0.851 (0.045)	0.842 (0.045)	0.810 (0.055)	0.814 (0.063)	0.755 (0.090)	0.819 (0.067)
DOY 201–230	0.767 (0.050)	0.769 (0.054)	0.767 (0.045)	0.718 (0.057)	0.718 (0.056)	0.680 (0.062)	0.736 (0.064)
DOY 231–260	0.752 (0.061)	0.818 (0.039)	0.819 (0.038)	0.799 (0.053)	0.767 (0.065)	0.717 (0.064)	0.779 (0.066)
DHP upward							
DOY 201–230	0.608 (0.127)	0.657 (0.070)	0.658 (0.057)	0.648 (0.057)	0.613 (0.063)	0.612 (0.064)	0.633 (0.080)
DOY 231–260	0.532 (0.115)	0.623 (0.078)	0.639 (0.049)	0.651 (0.046)	0.650 (0.048)	0.647 (0.044)	0.623 (0.080)

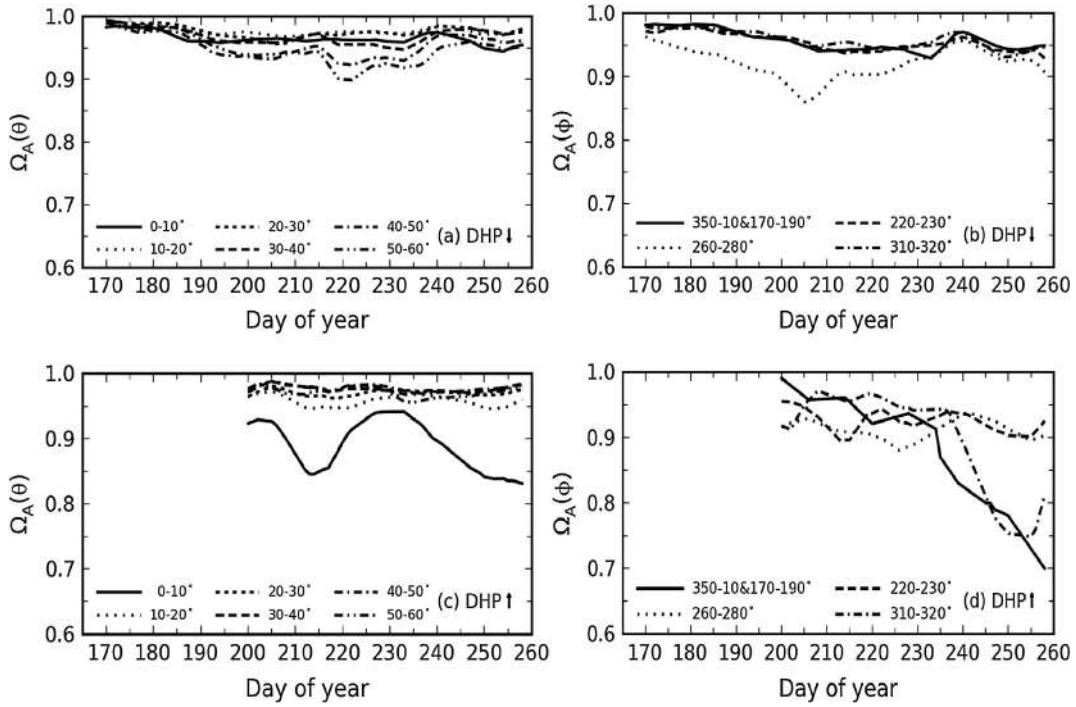

Fig. 5. Seasonal variation of $\Omega_A(\theta)$ and $\Omega_A(\phi)$ estimated from the downward (a and b) and upward (c and d) DHP observations. $\Omega_A(\phi)$ along 90° is not shown in (b) and (d) because of the operator shadow.

Table 3
The $\Omega_A(\theta)$ mean (standard deviation) values estimated from DHP for different view angles and periods of the season. The last column is an average all angular values. VZA: view zenith angles; DOY: day-of-year.

VZAs	0–10°	10–20°	20–30°	30–40°	40–50°	50–60°	Average
DHP downward							
DOY 170–200	0.971 (0.015)	0.982 (0.012)	0.982 (0.013)	0.977 (0.015)	0.965 (0.023)	0.968 (0.022)	0.974 (0.018)
DOY 201–230	0.963 (0.012)	0.973 (0.010)	0.969 (0.015)	0.960 (0.015)	0.936 (0.025)	0.928 (0.051)	0.955 (0.031)
DOY 231–260	0.961 (0.015)	0.977 (0.011)	0.978 (0.010)	0.970 (0.018)	0.958 (0.023)	0.944 (0.029)	0.965 (0.022)
DHP upward							
DOY 201–230	0.901 (0.055)	0.957 (0.017)	0.970 (0.014)	0.979 (0.012)	0.981 (0.011)	0.976 (0.015)	0.961 (0.038)
DOY 231–260	0.878 (0.055)	0.959 (0.023)	0.971 (0.012)	0.974 (0.012)	0.975 (0.010)	0.966 (0.014)	0.954 (0.043)

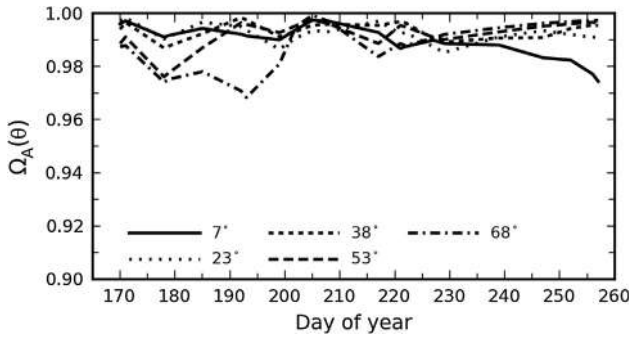

Fig. 6. Seasonal variation of $\Omega_A(\theta)$ estimated from LAI-2200 for different angular rings (Table A.1).

section level. The increase of the CIs values from $\Omega_A(\theta, \phi)$ to $\Omega_A(\theta)$ and $\Omega_A(\phi)$ and to $\Omega_A(\nu)$ is not unexpected because of the increase of canopy randomness with the segment size (Leblanc and Fournier, 2014; Pisek et al., 2011). The integration of the canopy architecture into rings or azimuth sections masks non-random gap distributions at small scales within the canopy and thus affects the ACI calculation. The differences between $\Omega_A(\theta, \phi)$ and $\Omega_A(\theta)$ reflect the reduction of canopy non-randomness because of the integration of cells into zenith rings.

4.1.2. Variation of CI with zenith angles

Both $\Omega_A(\theta, \phi)$ and $\Omega_A(\theta)$ can provide a fine explanation for the Ω change with zenith angles. Our results show a consistent decreasing trend of $\Omega_A(\theta, \phi)$ and $\Omega_A(\theta)$ with θ from DHP and LAI-2200, excluding 0–10° (Figs. 4–6). A consistent decreasing trend of Ω_{LX} with θ was also reported from DHP and LAI-2200 (Fang et al., 2014). The decreasing of Ω with θ is related to the gap size distribution (Chen, 1996; Kucharik et al., 1999; Ryu et al., 2010b). The regularly spaced rice crowns result in large gaps (high clumping) along the row direction at high viewing angles. Similar lower CI values for large θ have been observed for regularly spaced trees due to the large gap sizes between crowns (Kucharik et al., 1999). However, other studies have indicated that Ω generally increases with the view angle for boreal forests (Chen, 1996; Kucharik et al., 1999; Leblanc et al., 2005a), temperate forests (Kucharik et al., 1999; Macfarlane et al., 2007), grassland (Nouvellon et al., 2000), and maize crops (Demarez et al., 2008; Fang et al., 2018). Moreover, the angular variation of Ω is more complicated for a savannah ecosystem (Piayda et al., 2015; Ryu et al., 2010b). The variation of CI with θ should be further investigated for different vegetation types.

In field CI estimation, very low and high zenith angles are usually avoided because of higher uncertainties (Gonsamo and Pellikka, 2009; Walter et al., 2003). This study has revealed that $\Omega_A(\theta, \phi)$ or $\Omega_A(\theta)$ present higher variability for 0–10°, affected by the gap fraction

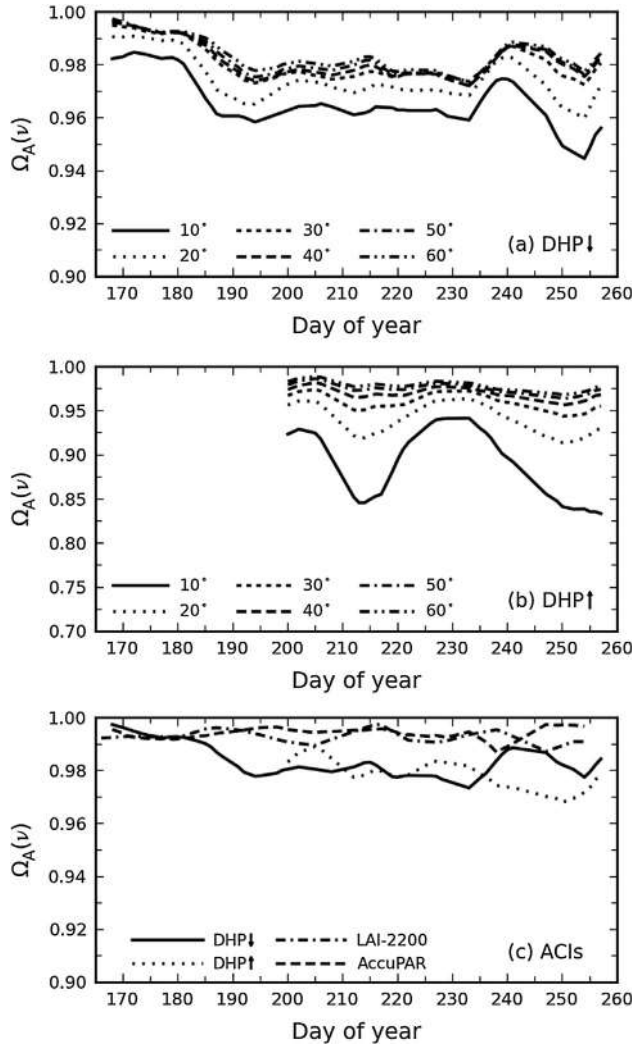

Fig. 7. Seasonal variation of $\Omega_A(\nu)$ estimated from the downward (a) and upward (b) DHP for different solid angles. Panel (c) compares $\Omega_A(\nu)$ estimated from DHP (ν = 60°), LAI-2200 (ν = 74.1°), and AccuPAR (ν = 90°).

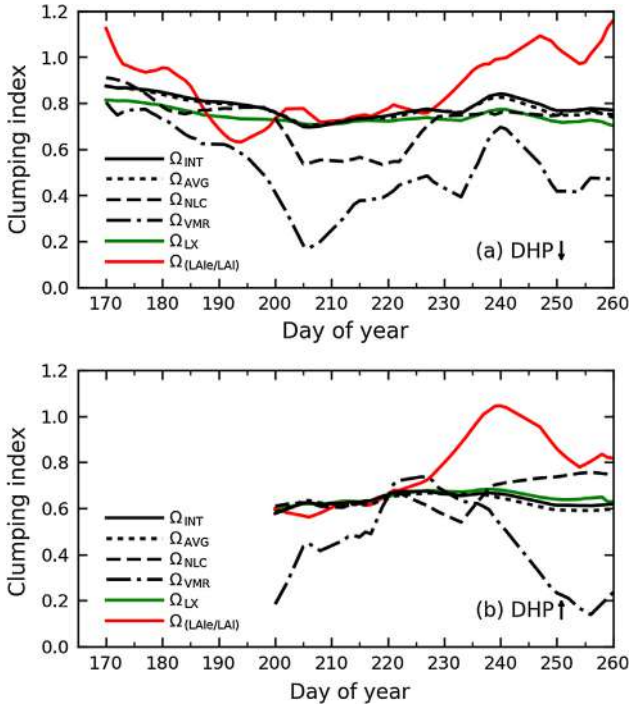

Fig. 8. Seasonal variation of the whole ACIs calculated from the directional $\Omega_A(\theta, \phi)$ (Fig. 4) for downward (a) and upward DHPs (b), respectively. Ω_{INT}, Ω_{AVG}, Ω_{NLC}, and Ω_{VMR} are from the integration, averaging, non-linear correction, and the variance-to-mean ratio methods. The Ω_{VMR} lines have been offset up by 0.2 (a) and 1.0 (b), respectively. The green and red lines show the average CIs calculated using the LX method (Ω_{LX}, Eq. (23)) and as a ratio of the DHP LAI_e to the destructive LAI (Eq. (1)).

Table 4
The whole ACIs estimated from DHP using the integration (INT), simple averaging (AVG), non-linear correction (NLC), and variance-to-mean ratio (VMR) methods for different periods of the season. The last two columns show the CIs estimated using the LX method (Ω_{LX}, Eq. (23)) and the ratio method (Ω (LAI_e/LAI), Eq. (1)).

	Ω_{INT}	Ω_{AVG}	Ω_{NLC}	Ω_{VMR}	Ω_{LX}	$\Omega(LAI_e/LAI)$
DHP downward						
DOY 170–200	0.824	0.819	0.803	0.257	0.767	0.832
DOY 201–230	0.736	0.736	0.595	−0.049	0.722	0.759
DOY 231–260	0.791	0.777	0.755	0.115	0.737	1.008
DHP upward						
DOY 201–230	0.639	0.634	0.623	−0.463	0.640	0.642
DOY 231–260	0.637	0.622	0.699	−0.613	0.658	0.910

variation close to the zenith (Figs. 4 and 5). Other studies also reported high gap fraction and CI uncertainties for forest types when θ > 70° (Kucharik et al., 1999). The high variability can be partly alleviated by sampling more observations. In practice, the 30–60° range is often used because of the small $\Omega(\theta)$ variation within this zenith range; thus the mean Ω for this range can represent the overall Ω (Duthoit et al., 2008; Gonsamo and Pellikka, 2009; Leblanc et al., 2005a). Some researchers recommended using the 55–60° range to estimate the whole CI because at this zenith range the G function is nearly independent of the leaf angle distribution (Gonsamo and Pellikka, 2009; Leblanc and Fournier, 2014). In particular, the LAI estimated from the 57.5° ($G(57.5°) \approx 0.5$) is found to be superior to those estimated from the Miller method (Eq. (3)) (Baret et al., 2010; Leblanc and Fournier, 2014).

Ω(0) indicates the distribution of canopy clumping at the nadir direction and is relevant to many nadir observation sensors such as the Landsat sensors. Ω(0) can be derived through numerical radiative transfer simulation (Chen et al., 2008) or estimated based on an empirical relationship between $\Omega(\theta)$ and θ (Fang et al., 2014). The DHP (θ = 0–10°) and LAI-2200 (θ = 7°) observations presented in Figs. 4–6 are close to the nadir Ω(0). In theory, Ω(0) can be measured with the TRAC instrument in the tropical area when the sun is at the overhead direction. Ω(0) can also be estimated through an allometric equation with canopy structure parameters, e.g., crown porosity and foliage projection cover estimated from cover photography (Chianucci et al., 2016; Macfarlane et al., 2007; Ryu et al., 2012). In some occasions the CI estimated from low zenith angles was used to represent the overall Ω (Ryu et al., 2012).

4.1.3. Variation of CI with azimuth angles

Generally, it is assumed that most plants have azimuth symmetry so that the clumping effect only deals with leaf inclination distribution. Our study in rice crops shows that $\Omega_A(\theta, \phi)$ and $\Omega_A(\phi)$ are not rotationally symmetric and their values depend on the azimuth direction. Clear investigation of $\Omega_A(\theta, \phi)$ and $\Omega_A(\phi)$ requires that all DHP measurement should be fixed on a particular azimuth direction. $\Omega_A(\theta, \phi)$ estimated from the downward DHP shows a higher clumping effect along the row direction (Figs. 4b and 5b), whereas the upward DHP shows a higher clumping effect along the cross-row direction (Fig. 5d). The different performances of the DHP may be caused by the different view directions and gap distributions. Earlier studies about the leaf

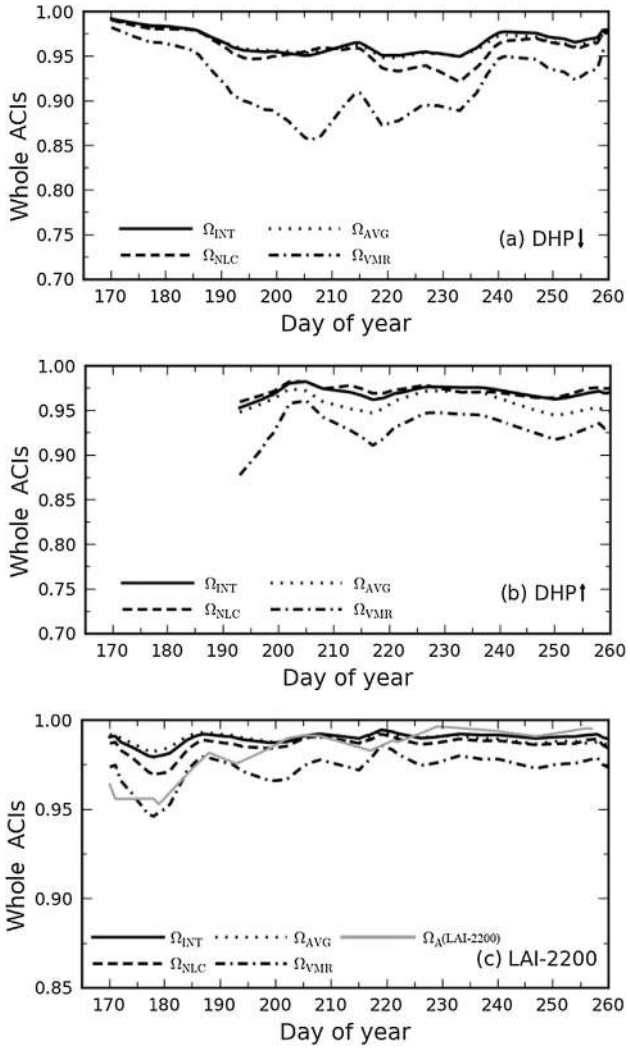

Fig. 9. Seasonal variation of the whole ACIs calculated from $\Omega_A(\theta)$ for downward DHP (a), upward DHP (b), and LAI-2200 (c). Ω_{INT}, Ω_{AVG}, Ω_{NLC}, and Ω_{VMR} are the same as in Fig. 8. The gray line in (c) shows the whole ACI reported in the LAI-2200 data file (Eq. (10)).

Table 5
The whole ACIs estimated from LAI-2200 using the INT, AVG, NLC, and VMR methods for different periods of the season. The last column shows the ACI reported in the LAI-2200 data file.

DOYs	Ω_{INT}	Ω_{AVG}	Ω_{NLC}	Ω_{VMR}	Ω_A(LAI-2200)
170–200	0.987	0.989	0.982	0.966	0.969
201–230	0.991	0.990	0.989	0.976	0.989
231–260	0.991	0.989	0.988	0.977	0.994

azimuth variation have reported that departure from the random distribution mainly occurs at the row and cross-row directions (Cohen and Fuchs, 1987; Sinoquet and Andrieu, 1993). The variability of CI with zenith and azimuth angles complicates the estimation of the whole CI, and should be further investigated for different vegetation types, especially for row crops.

4.1.4. $\Omega_A(\nu)$ and CI variation at the landscape level

$\Omega_A(\nu)$ allows all gap fractions to contribute equally to the calculation of the foliage distribution in a solid angle 4ν. Fig. 7 shows that the $\Omega_A(\nu)$ values are close to unity and the rice canopies show little clumping at larger scales, especially during the beginning of the season. This phenomenon has also been demonstrated by previous studies (Chianucci and Cutini, 2013; Chianucci et al., 2015). The consistency of the $\Omega_A(\nu)$ values also shows the robustness of the three instruments for CI estimation at the landscape scale. The slight differences in the second half of the season are mainly attributed to the different viewing fields of the instruments.

4.2. Directional and whole ACI metrics

Current CI studies usually distinguish different levels of canopy clumping at shoot, stand, and landscape scales (Norman and Jarvis, 1974; Stenberg et al., 2014). Clumping effects at different canopy levels are physically important but difficult to quantify with optical methods (Stenberg et al., 2014). The ACIs are easy to quantify with optical methods and can be easily adopted in radiative transfer and land surface models. Fig. 8 shows that the $\Omega_A(\theta, \phi)$ and Ω_{LX} are numerically similar for rice crops. Indeed, the Ω_{LX} can be considered as another form of ACI over the entire segments, while the $\Omega_A(\theta, \phi)$ indicates the foliage distribution over a particular direction (θ, ϕ). $\Omega_A(\theta, \phi)$, $\Omega_A(\theta)$, and $\Omega_A(\phi)$ can be used to study foliage angular distribution pattern at different levels, while $\Omega_A(\nu)$ approximates ACI at the landscape level. However, $\Omega_A(\theta)$, $\Omega_A(\phi)$, and $\Omega_A(\nu)$ are unable to characterize the overall foliage clumping because the canopy segment size requirement for CI calculation (Eq. (7)) is often smaller than a ring, an azimuth sector and a solid angle. The combined use of all ACI metrics allows a more comprehensive assessment of the true canopy LAI (Eq. (8)).

The whole ACI can be calculated from the directional ACIs and the directional gap fractions (Section 2.3). Among the four methods to calculate the whole ACI, the INT and AVG methods agree very well and are robust over the season (Figs. 8 and 9). The NLC method can approximate the INT and AVG methods very well, but is easily affected by outlying gap fraction values. The VMR method is indicative of the seasonal ACI variation but gives systematically lower values. The whole ACIs calculated from LAI-2200 are on par with the values reported in LAI-2200 using Eq. (10) (Fig. 9).

4.3. Optical instruments for CI measurement

4.3.1. DHP

DHP provides a far finer directional spatial sampling of canopy gaps than other optical instruments, allowing CI to be derived along multiple zenith and azimuth angles (Garrigues et al., 2008). The entire DHP image over $0 - 90^\circ$ is required to provide the most accurate estimate of $\Omega_A(\theta, \phi)$. However, the entire DHP FOV is rarely utilized in data analysis, due to multiple factors affecting the classification accuracy for large zenith angles (Jonckheere et al., 2004; Leblanc et al., 2005a). Therefore, it is common practice to restrict the instrument FOV to a maximum zenith angle for CI estimation (Sea et al., 2011); for example, the 0–60° range used in this study. On the other hand, the whole ACI does not equal to the overall ACI for 0–90° because of the view angle restriction (< 60°). Other studies found that a discrete narrow zenith angle range around 55–60° also provides good CI and LAI estimates (Baret et al., 2010; Leblanc and Fournier, 2014).

A stable azimuth angle in DHP measurement assists the directional CI estimation and comparison. The accuracy of CI estimation from DHP is dependent on the accuracy of a classification procedure that involves a subjective determination of plant pixels and gaps. The upward DHP observations, generally placed between rows, are subject to higher uncertainties because of the high probability of obtaining zero gap fractions for short canopies.

4.3.2. LAI-2200

The $\Omega_A(\theta)$ and $\Omega_A(\nu)$ values estimated from LAI-2200 are similarly high (> 0.97) (Figs. 6 and 7), although they represent canopy non-randomness at different levels. In this study, the $P(\theta)$ value represents the mean $P(\theta, \phi)$ value within a 270° view because of the view cap

applied. The ACI values generally increase when larger view caps are fitted with the instrument (Chianucci et al., 2015; Nilson et al., 2011; Ryu et al., 2010a). The large view caps are recommended for sparse canopies and for the LAI_e estimation, whereas the narrow view caps are for dense canopies and for the LAI estimation (Chianucci et al., 2015; Kobayashi et al., 2013). Chianucci et al. (2015) reported that ACI agrees best with the reference CI when a narrow 10° view cap is used for a deciduous broadleaf forest. Applying a 10° view cap for LAI-2200, although difficult to align in practice, may be able to mimic the $\Omega_A(\theta, \phi)$ estimation from DHP.

4.3.3. AccuPAR

The AccuPAR $\Omega_A(\nu)$ indicates the foliage non-randomness in horizontal directions, because of the angular integration in the observation bins ($\nu = 90°$). The large view angle and $\Omega_A(\nu)$ for the upper hemisphere make AccuPAR attractive for spatial homogeneity investigation. The AccuPAR $\Omega_A(\nu)$ is calculated over n segments, which are assumed to have random gap and foliage distributions within them. Further improvement can be obtained by using measurements from the 80 pins and segmenting the AccuPAR's probe into smaller groups (Peper and McPherson, 1998). Assuming the area sampled by a group is relatively random, an improved $\Omega_A(\nu)$ can be estimated using the LX method (Eq. (23)).

4.3.4. Other indirect methods

Other researchers have used upward-looking digital cameras to estimate continuous CI for forests (Ryu et al., 2012), and downward-looking cameras for crop Ω_A (Li et al., 2015). Qu et al. (2014) designed a multi-point linear array of optical sensors (MLAOS) for continuous clumping measurement. Using both above and below canopy optical sensors, MLAOS measures the canopy transmittance and calculates gap fractions using a 650 nm band-pass filter in sunlit conditions. MLAOS has been successfully used to estimate $\Omega_A(\nu)$ for a deciduous needle-leaf forest (DNF) in northeast China. Compared to our values in the rice field (Fig. 7), the $\Omega_A(\nu)$ values are much lower for DNF (0.6–0.9) (Qu et al., 2014), which may be related to the spatial heterogeneity caused by the selective logging at the DNF site.

Although not used in this study, TRAC is another popular method for canopy CI characterization using the gap size distribution theory (Chen and Cihlar, 1995). TRAC records the transmitted direct light along a transect using PAR sensors. The canopy gap size distribution for a particular solar direction is then calculated. The differences between the field measured and theoretically random gap size distributions are used to quantify the clumping effect (Chen and Cihlar, 1995). With Eq. (23), the $\Omega_A(\nu = 90°)$ may be calculated from TRAC using gap fractions for the upper hemisphere obtained by the PAR sensors. With a masked measurement, the direct transmittance obtained by TRAC can be used to estimate $\Omega_A(\theta, \phi)$ (Eq. (9)). Furthermore, the theoretical basis introduced in section 2 may be extended to calculate the directional and whole ACIs based on the gap size distribution method.

4.4. Implications

The variation of canopy clumping in angles and space is critical for models attempting to map radiation fields inside the canopy. Assumptions about isotropic clumping indices, for which standard radiative transfer models are typically used, remain large sources of uncertainty in canopy reflectance simulation (Wang and Li, 2013). Earlier studies and our results indicate that in most cases CI is anisotropic. Several ecological models have already been developed to allow for clumping variation with positions in the canopy (Sinoquet, 1993). The directional ACI metrics can be incorporated into ecological models to investigate the effect of angular clumping on light interception at various scales. Angular CI from field measurements could help improve light interactions and directional reflectance simulations in heterogeneous canopies with turbid radiative transfer models. Conversely, Duthoit et al. (2008) showed that the improvement of canopy directional reflectance simulation using angularly variable CI was marginal (< 3–5%) and suggested using the mean CI to simplify the RT model. To what extent this could lead to better reflectance simulation and parameter retrieval by inversion of remote sensing data is still a matter of concern and further investigation.

While the CI can be theoretically derived in simulation studies (Duthoit et al., 2008; Leblanc and Fournier, 2014), the ACI can be practically obtained through optical measurements. It is not straightforward to equal the CI (Eq. (1)) with the spatial distribution of foliage elements. Many foliage distribution metrics have been investigated and found useful, such as the fractional dimension method (Foroutan-pour et al., 1999; Jonckheere et al., 2006; Nackaerts et al., 1999), the Pielou's coefficient of segregation (PCS) (Pisek et al., 2011; Walter et al., 2003), and the standardized Morisita's index (SMI) (García et al., 2015; Krebs, 1999). However, accurate positioning of foliage elements in the field is a difficult and time consuming process.

5. Conclusion

This study proposes several expanded apparent clumping indices (ACIs) that can be obtained in field optical measurements using DHP, LAI-2200, and AccuPAR. Using the same logarithmic gap fraction averaging method, the ACI metrics expand the theoretical CI and is beneficial for more accurate LAI estimation (Eq. (8)). Among the ACI metrics, $\Omega_A(\theta, \phi)$ indicates the foliage non-random distribution at direction (θ, ϕ), while $\Omega_A(\theta)$ and $\Omega_A(\phi)$ represent the foliage distribution over a concentric ring and an azimuth sector, respectively. $\Omega_A(\nu)$ describes the foliage spatial distribution over a landscape. Currently, only $\Omega_A(\theta)$ is being reported by LAI-2200. This paper shows that all ACI metrics can be derived from DHP at different resolutions, whereas both $\Omega_A(\theta)$ and $\Omega_A(\nu)$ can be estimated from LAI-2200, and $\Omega_A(\nu)$ from AccuPAR.

For paddy rice fields, the directional ACI values generally increase with the increasing segment size, in the order of $\Omega_A(\theta, \phi) < \Omega_A(\theta)$ and $\Omega_A(\phi) < \Omega_A(\nu)$. The ACI values also decrease with the zenith angles and are not azimuthally symmetric, especially at the row and cross-row directions. The whole ACI calculated with the integration method (Ω_{INT}) can be well approximated using a simple averaging (Ω_{AVG}) or a non-linear correction (Ω_{NLC}) method. The variance-to-mean ratio (Ω_{VMR}) method can be used as a convenient indicator of the general ACI variation. The expanded ACI metrics can be used to improve the estimation of the LAI_e and other canopy biophysical parameters from remote sensing data. Further studies can be performed for other vegetation ecosystems, especially the heterogeneous areas.

Acknowledgments

This study was supported by the National Natural Science Foundation of China (41471295, 41171333) and the Hundred Talent Program of the Chinese Academy of Sciences. Ms. L. Ma helped with the figures. We would like to thank the interns who attended the field work at various stages, and the farmers for allowing us to make use of their fields for in situ measurements.

Appendix A

A.1 The ring range and weighting factors for LAI-2200 (LI-COR, 2010).

Ring #	Ring center	Nominal range	Weights
1	7°	0.0–12.3°	0.041
2	23°	16.7–28.6°	0.131
3	38°	32.4–43.4°	0.201
4	53°	47.3–58.1°	0.290
5	68°	62.3–74.1°	0.337

A.2 List of symbols used in the paper

Symbol	Description
θ	zenith angle
ϕ	azimuth angle
ν	solid angle
G(θ)	the fraction of foliage projected in the direction θ
G(0)	the fraction of foliage projected at the vertical direction ($\theta = 0°$)
$P(\theta)$	canopy gap fraction at direction θ
$P(\phi)$	canopy gap fraction at direction ϕ
$P(\nu)$	canopy gap fraction at solid angle ν
$P(0)$	gap fraction at the vertical direction ($\theta = 0°$)
Ω	Clumping index (CI), defined as LAI_e/LAI
Ω_A	Apparent clumping index (ACI)
$\Omega_A(\theta, \phi)$	ACI at direction (θ, ϕ)
$\Omega_A(\theta)$	ACI for a conic ring at zenith angle θ
$\Omega_A(\phi)$	ACI for an azimuth sector at direction ϕ
$\Omega_A(\nu)$	ACI calculated for a solid viewing angle ν
Ω_{LX}	CI derived by the LX method

Appendix B. Supplementary material

Supplementary data associated with this article can be found, in the online version, at https://doi.org/10.1016/j.isprsjprs.2018.06.022.

References

Baret, F., de Solan, B., Lopez-Lozano, R., Ma, K., Weiss, M., 2010. GAI estimates of row crops from downward looking digital photos taken perpendicular to rows at 57.5° zenith angle: theoretical considerations based on 3D architecture models and application to wheat crops. Agric. For. Meteorol. 150 (11), 1393–1401.

Chen, B., et al., 2016. Assessment of foliage clumping effects on evapotranspiration estimates in forested ecosystems. Agric. For. Meteorol. 216, 82–92.

Chen, J.M., 1996. Optically based methods for measuring seasonal variation of leaf area index in boreal conifer stands. Agric. For. Meteorol. 80 (2–4), 135–163.

Chen, J.M., Cihlar, J., 1995. Plant canopy gap-size analysis theory for improving optical measurements of leaf-area index. Appl. Opt. 34, 6211–6222.

Chen, J.M., Menges, C.H., Leblanc, S.G., 2005. Global mapping of foliage clumping index using multi-angular satellite data. Rem. Sens. Environ. 97 (4), 447–457.

Chen, J.M., et al., 2012. Effects of foliage clumping on the estimation of global terrestrial gross primary productivity. Global Biogeochem. Cycles 26 (1), GB1019. http://dx.doi.org/10.1029/2010gb003996.

Chen, Q., Baldocchi, D., Gong, P., Dawson, T., 2008. Modeling radiation and photosynthesis of a heterogeneous savanna woodland landscape with a hierarchy of model complexities. Agric. For. Meteorol. 148 (6–7), 1005–1020.

Chianucci, F., Cutini, A., 2013. Estimation of canopy properties in deciduous forests with digital hemispherical and cover photography. Agric. For. Meteorol. 168, 130–139.

Chianucci, F., et al., 2016. Estimation of canopy attributes in beech forests using true colour digital images from a small fixed-wing UAV. Int. J. Appl. Earth Obs. Geoinf. 47, 60–68.

Chianucci, F., Macfarlane, C., Pisek, J., Cutini, A., Casa, R., 2015. Estimation of foliage clumping from the LAI-2000 Plant Canopy Analyzer: effect of view caps. Trees-Struct. Funct. 29 (2), 355–366.

Cohen, S., Fuchs, M., 1987. The distribution of leaf area, radiation, photosynthesis and transpiration in a Shamouti orange hedgerow orchard. Part I. Leaf area and radiation. Agric. For. Meteorol. 40 (2), 123–144.

Decagon Devices, Inc., 2004. AccuPAR PAR/LAI ceptometer (model LP-80) Operator's Manual, Version 1.2, Pullman, WA 99162, USA.

Demarez, V., Duthoit, S., Baret, F., Weiss, M., Dedieu, G., 2008. Estimation of leaf area and clumping indexes of crops with hemispherical photographs. Agric. For. Meteorol. 148 (4), 644–655.

Drouet, J.L., Moulia, B., 1997. Spatial re-orientation of maize leaves affected by initial plant orientation and density. Agric. For. Meteorol. 88, 85–100.

Duthoit, S., Demarez, V., Gastellu-Etchegorry, J.-P., Martin, E., Roujean, J.-L., 2008. Assessing the effects of the clumping phenomenon on BRDF of a maize crop based on 3D numerical scenes using DART model. Agric. For. Meteorol. 148 (8–9), 1341–1352.

Fang, H., Li, W., Wei, S., Jiang, C., 2014. Seasonal variation of leaf area index (LAI) over paddy rice fields in NE China: intercomparison of destructive sampling, LAI-2200, digital hemispherical photography (DHP), and AccuPAR methods. Agric. For. Meteorol. 198–199, 126–141.

Fang, H., Ye, Y., Liu, W., Wei, S., Ma, L., 2018. Continuous estimation of canopy leaf area index (LAI) and clumping index over broadleaf crop fields: an investigation of the PASTIS-57 instrument and smartphone applications. Agric. For. Meteorol. 253–254, 48–61.

Fernandes, R., et al., 2014. Global leaf area index product validation good practices. Version 2. https://lpvs.gsfc.nasa.gov/LAI/LAI_home.html.

Foroutan-pour, K., Dutilleul, P., Smith, D.L., 1999. Soybean canopy development as affected by population density and intercropping with corn: fractal analysis in comparison with other quantitative approaches. Crop Sci. 39 (6), 1784–1791.

García, M., et al., 2015. Canopy clumping appraisal using terrestrial and airborne laser scanning. Rem. Sens. Environ. 161, 78–88.

Garrigues, S., et al., 2008. Intercomparison and sensitivity analysis of leaf area index retrievals from LAI-2000, AccuPAR, and digital hemispherical photography over croplands. Agric. For. Meteorol. 148, 1193–1209.

Gonsamo, A., Pellikka, P., 2009. The computation of foliage clumping index using hemispherical photography. Agric. For. Meteorol. 149 (10), 1781–1787.

Gonsamo, A., Walter, J.-M.N., Pellikka, P., 2010. Sampling gap fraction and size for estimating leaf area and clumping indices from hemispherical photographs. Can. J. For. Res. 40 (8), 1588–1603.

Haverd, V., et al., 2012. The canopy semi-analytic pgap and radiative transfer

(CanSPART) model: formulation and application. Agric. For. Meteorol. 160, 14–35.
He, L., Chen, J.M., Pisek, J., Schaaf, C.B., Strahler, A.H., 2012. Global clumping index map derived from the MODIS BRDF product. Rem. Sens. Environ. 119, 118–130.
He, L., et al., 2016. Inter- and intra-annual variations of clumping index derived from the MODIS BRDF product. Int. J. Appl. Earth Obs. Geoinf. 44, 53–60.
Jonckheere, I., et al., 2004. Review of methods for in situ leaf area index determination Part I. Theories, sensors and hemispherical photography. Agric. For. Meteorol. 121 (1–2), 19–35.
Jonckheere, I., Nackaerts, K., Muys, B., van Aardt, J., Coppin, P., 2006. A fractal dimension-based modelling approach for studying the effect of leaf distribution on LAI retrieval in forest canopies. Ecol. Model. 197 (1–2), 179–195.
Kobayashi, H., Ryu, Y., Baldocchi, D.D., Welles, J.M., Norman, J.M., 2013. On the correct estimation of gap fraction: how to remove scattered radiation in gap fraction measurements? Agric. For. Meteorol. 174–175, 170–183.
Krebs, C.J., 1999. Ecological Methodology. Benjamin/Cummings, Menlo Park, California.
Kucharik, C.J., Norman, J.M., Gower, S.T., 1999. Characterization of radiation regimes in non-random forest canopies: theory, measurements, and simplified modeling approach. Tree Physiol. 19, 695–706.
Lang, A.R.G., 1986. Leaf area and average leaf angle from transmission of direct sunlight. Aust. J. Bot. 34, 349–355.
Lang, A.R.G., Xiang, Y., 1986. Estimation of leaf area index from transmission of direct sunlight in discontinuous canopies. Agric. For. Meteorol. 37 (3), 229–243.
Leblanc, S.G., Chen, J.M., Fernandes, R., Deering, D.W., Conley, A., 2005a. Methodology comparison for canopy structure parameters extraction from digital hemispherical photography in boreal forests. Agric. For. Meteorol. 129 (3–4), 187–297.
Leblanc, S.G., et al., 2005b. Canada-wide foliage clumping index mapping from multi-angular POLDER measurements. Can. J. Rem. Sens. 31 (5), 364–376.
Leblanc, S.G., Fournier, R.A., 2014. Hemispherical photography simulations with an architectural model to assess retrieval of leaf area index. Agric. For. Meteorol. 194, 64–76.
LI-COR, Inc., 2010. LAI-2200 Plant Canopy Analyzer: Instruction Manual, pp. 10–23.
Li, X.H., et al., 2015. The design and implementation of the leaf area index sensor. Sensors 15 (3), 6250–6269.
Macfarlane, C., et al., 2007. Estimation of leaf area index in eucalypt forest using digital photography. Agric. For. Meteorol. 143 (3–4), 176–188.
Miller, J.B., 1967. A formula for average foliage density. Aust. J. Bot 15, 141–144.
Nackaerts, K., Sterckx, S., Coppin, P., 1999. Fractal dimension as correction factor for stand-level indirect leaf area index measurements. In: Proc. SPIE 3868, Remote Sensing for Earth Science, Ocean, and Sea Ice Applications, pp. 80–89. https://doi.org/10.1117/12.373083.
Ni-Meister, W., Yang, W., Kiang, N.Y., 2010. A clumped-foliage canopy radiative transfer model for a global dynamic terrestrial ecosystem model. I: Theory. Agric. For. Meteorol. 150 (7–8), 881–894.
Nilson, T., 1971. A theoretical analysis of the frequency of gaps in plant stands. Agric. Meteorol. 8, 25–38.
Nilson, T., Kuusk, A., Lang, M., Pisek, J., Kodar, A., 2011. Simulation of statistical characteristics of gap distribution in forest stands. Agric. For. Meteorol. 151 (7), 895–905.
Norman, J.M., Jarvis, P.G., 1974. Photosynthesis in Sitka spruce (Picea sitchensis (Bong.) Carr.). III. Measurements of canopy structure and interception of radiation. J. Appl. Ecol. 11 (1), 375–398.
Nouvellon, Y., et al., 2000. PAR extinction in shortgrass ecosystems: effects of clumping, sky conditions and soil albedo. Agric. For. Meteorol. 105 (1–3), 21–41.
Peper, P.J., McPherson, E.G., 1998. Comparison of five methods for estimating leaf area index of open grown deciduous trees. J. Arboric. 24 (2), 98–111.
Piayda, A., et al., 2015. Influence of woody tissue and leaf clumping on vertically resolved leaf area index and angular gap probability estimates. For. Ecol. Manage. 340, 103–113.
Pinty, B., et al., 2006. Simplifying the interaction of land surfaces with radiation for relating remote sensing products to climate models. J. Geophys. Res. 111 (D02116).
Pisek, J., Lang, M., Nilson, T., Korhonen, L., Karu, H., 2011. Comparison of methods for measuring gap size distribution and canopy nonrandomness at Järvselja RAMI (RAdiation transfer Model Intercomparison) test sites. Agric. For. Meteorol. 151 (3), 365–377.
Pisek, J., et al., 2013. Retrieving vegetation clumping index from Multi-angle Imaging SpectroRadiometer (MISR) data at 275 m resolution. Rem. Sens. Environ. 138, 126–133.
Qu, Y., Fu, L., Han, W., Zhu, Y., Wang, J., 2014. MLAOS: a multi-point linear array of optical sensors for coniferous foliage clumping index measurement. Sensors 14 (5), 9271–9289.
Rambal, S., et al., 2003. Drought controls over conductance and assimilation of a Mediterranean evergreen ecosystem: scaling from leaf to canopy. Glob. Change Biol. 9 (12), 1813–1824.
Ryu, Y., et al., 2010a. On the correct estimation of effective leaf area index: does it reveal information on clumping effects? Agric. For. Meteorol. 150 (3), 463–472.
Ryu, Y., et al., 2010b. How to quantify tree leaf area index in an open savanna ecosystem: a multi-instrument and multi-model approach. Agric. For. Meteorol. 150, 63–76.
Ryu, Y., et al., 2012. Continuous observation of tree leaf area index at ecosystem scale using upward-pointing digital cameras. Rem. Sens. Environ. 126, 116–125.
Sea, W.B., et al., 2011. Documenting improvement in leaf area index estimates from MODIS using hemispherical photos for Australian savannas. Agric. For. Meteorol. 151 (11), 1453–1461.
Sinoquet, H., 1993. Modelling radiative transfer in heterogeneous canopies and intercropping systems. In: Varlet-Grancher, C., Bonhomme, R., Sinoquet, H. (Eds.), Crop Structure and Light Microclimate, Characterization and Applications. INRA, Paris, pp. 229–252.
Sinoquet, H., Andrieu, B., 1993. The geometrical structure of plant canopies: characterization and direct measurement methods. In: Varlet-Grancher, C., Bonhomme, R., Sinoquet, H. (Eds.), Crop Structure and Light Microclimate: Characterization and Applications. INRA, Paris, pp. 131–158.
Stenberg, P., Mõttus, M., Rautiainen, M., Sievänen, R., 2014. Quantitative characterization of clumping in Scots pine crowns. Ann. Bot. 114 (4), 689–694.
van Gardingen, P.R., Jackson, G.E., Hernandez-Daumas, S., Russell, G., Sharp, L., 1999. Leaf area index estimates obtained for clumped canopies using hemispherical photography. Agric. For. Meteorol. 94 (3–4), 243–257.
Walter, J.-M.N., Fournier, R.A., Soudani, K., Meyer, E., 2003. Integrating clumping effects in forest canopy structure: an assessment through hemispherical photographs. Can. J. Rem. Sens. 29 (3), 388–410.
Wang, Q., Li, P., 2013. Canopy vertical heterogeneity plays a critical role in reflectance simulation. Agric. For. Meteorol. 169, 111–121.
Wei, S., Fang, H., 2016. Estimation of canopy clumping index from MISR and MODIS sensors using the normalized difference hotspot and darkspot (NDHD) method: the influence of BRDF models and solar zenith angle. Rem. Sens. Environ. 187, 476–491.
Weiss, M., Baret, F., 2010. CAN-EYE V6.1 User Manual.
Weiss, M., Baret, F., 2014. CAN-EYE V6.313 User Manual.
Woodgate, W., et al., 2016. Quantifying the impact of woody material on leaf area index estimation from hemispherical photography using 3D canopy simulations. Agric. For. Meteorol. 226–227, 1–12.
Yang, W., et al., 2010. A clumped-foliage canopy radiative transfer model for a Global Dynamic Terrestrial Ecosystem Model II: comparison to measurements. Agric. For. Meteorol. 150 (7–8), 895–907.